Coulomb blockade, current and shot noise in parallel double metallic quantum dot structures

2007 J. Phys.: Condens. Matter 19 026220

(http://iopscience.iop.org/0953-8984/19/2/026220)

INSTITUTE OF PHYSICS PUBLISHING JOURNAL OF PHYSICS: CONDENSED MATTER

J. Phys.: Condens. Matter **19** (2007) 026220 (11pp) doi:10.1088/0953-8984/19/2/026220

Coulomb blockade, current and shot noise in parallel double metallic quantum dot structures

V Hung Nguyen and V Lien Nguyen[1]

Theoretical Department, Institute of Physics, VAST, PO Box 429 Bo Ho, Hanoi 10000, Vietnam

E-mail: nvlien@iop.vast.ac.vn

Received 22 September 2006
Published 15 December 2006
Online at stacks.iop.org/JPhysCM/19/026220

Abstract

We systematically study sequential electron tunnelling through parallel double metallic quantum dot structures, focusing on the role of inter-dot coupling and parameter asymmetry. It is shown that the evolution of Coulomb blockade charging diagrams, induced by only the inter-dot capacitance, describes the existing experimental data quite well. Both the inter-dot capacitance and the resistance strongly affect the shot noise, making it super-Poissonian even in fully symmetric structures. An asymmetry of parameters, enhancing the role of inter-dot coupling, may produce a variety of current–voltage characteristics behaviours, including negative differential conductance regions, and a very large noise. For all structures studied the noise is shown to be more sensitive than the conductance to the inter-dot coupling as well as the parameter asymmetry.

(Some figures in this article are in colour only in the electronic version)

1. Introduction

Single electron devices such as single electron transistor (SET) or single electron pump (SEP) have attracted much attention from the early days of nanophysics [1, 2]. Due to a strong Coulomb effect these devices can carry a current only at bias voltages higher than some value called the Coulomb blockade (CB) threshold. For SETs (figure 1(b)), though the current–voltage (I–V) characteristics may have a staircase form when the difference between two tunnel resistances, coupling the metallic quantum dot (QD) to leads, is large enough (asymmetric SETs) [1], the differential conductance is never negative and the shot noise power S is always smaller than the full (Poissonian) shot noise value, $2eI$, where e is the elementary charge and I is the average current [3–5]. For SEPs, where two QDs are coupled in series (figure 1(c)) and the coupling between them plays an important role, the I–V curve may show

[1] Author to whom any correspondence should be addressed.

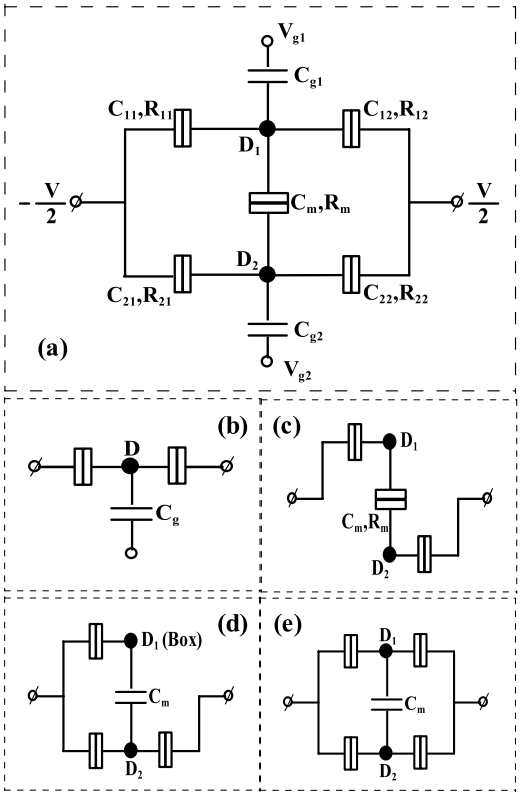

Figure 1. Equivalent circuit diagrams: general structure of parallel double QD (a) and particular configurations, SET (b), SEP (c), SET-Box (d) and the particular symmetric configuration to be examined (e).

a variety of behaviours, including regions of negative differential conductance (NDC) [6, 7]. The shot noise in these devices is, however, still always smaller than the Poissonian value (sub-Poissonian noise with Fano factor $F_n = S/2eI < 1$) [8]. Particularly, in the device drawn in figure 1(d) and experimentally investigated in [9] the presence of an electronic box, capacitively coupled with the SET, produces a richness of behaviours of both current and noise. It was shown [10] that the box may induce an electron accumulation in QDs, which in turn may cause noise enhancement. Depending on the box parameters, a very large (super-Poissonian, $F_n > 1$) noise may be observed even in regions of positive differential conductance.

Actually, as demonstrated in figure 1, all three devices mentioned above can be regarded as particular configurations of the parallel double quantum dot structure (PDQDS) drawn in figure 1(a). While the SEP (figure 1(c)) or the SET-Box (figure 1(d)) is the limiting asymmetric configuration, deduced from this PDQDS by removing two junctions ($\bar{1}2$ and $2\bar{1}$) or one junction ($\bar{1}2$), respectively, the most interesting limiting symmetric configuration is drawn in figure 1(e), where two QDs are capacitively coupled but there is no electron tunnelling between them. All other particular symmetric configurations are practically equivalent to (effective) SETs. Recently, PDQDSs have become very attractive in both fundamental (e.g. interference or Kondo effects [11–14]) and applied (e.g. quantum information [15–17]) investigations. In particular, transport properties of the PDQDS like that in figure 1(a) in the CB-regime have been experimentally examined in [18–20], where the CB-charging diagrams are analysed in detail.

The structure in figure 1(e) has also been measured in [21]. Theoretically, despite the SET as well as the SEP and the SET-Box having been thoroughly investigated [1–10], to the best of our knowledge the understanding, at least of the noise, is still very limited for the PDQDSs in figures 1(a) or (e). That is the reason behind the present work, where we systematically study sequential electron tunnelling characteristics in the PDQDSs mentioned. The charging diagram and the threshold voltage, characterizing the CB-phenomenon, will be examined in detail and the current and noise will be calculated using the master equation approach.

The paper is organized as follows. Section 2 is devoted to formulating the problem and presenting fundamental expressions. In section 3 the numerical results of the charging diagram, the I–V characteristics and the noise are presented and discussed. A brief summary is given in section 4.

2. Formulation of the problem and the method of calculation

Within the framework of the orthodox theory [2] the state $|i\rangle$ of the structure under study (see figure 1(a)) is entirely determined by the numbers of excess electrons in two QDs, $n_1^{(i)}$ in D_1 and $n_2^{(i)}$ in D_2. At a given (n_1, n_2)-state, the free energy of the system has the form:

$$F(n_1,n_2) = Q_1^2/2C_1^* + Q_2^2/2C_2^* + Q_1Q_2/C_m^* - (C_{11}+C_{12}+C_{21}+C_{22})V^2/4 - (C_{g1}V_{g1}^2 + C_{g2}V_{g2}^2)/2 + (n_1 - n_r)eV/2, \quad (1)$$

where $Q_1 = n_1e + C_{g1}V_{g1} + (C_{12}-C_{11})V/2$, $Q_2 = n_2e + C_{g2}V_{g2} + (C_{22}-C_{21})V/2$, $C_1^* = \Sigma/(C_{21}+C_{22}+C_{g2}+C_m)$, $C_2^* = \Sigma/(C_{11}+C_{12}+C_{g1}+C_m)$, $C_m^* = \Sigma/C_m$ with $\Sigma = (C_{11}+C_{12}+C_{g1}+C_m)(C_{21}+C_{22}+C_{g2}+C_m) - C_m^2$ and $n_1(n_r)$ is the number of electrons that have entered the device from the left (right) lead. Any electron transfer across junctions results in a change in free energy F. In the system of interest there are 10 possible sequential electron transfers across four arm-junctions ($1\bar{1}$, $1\bar{2}$, $2\bar{1}$ and $2\bar{2}$) to the right (+) or the left (−) and across the inter-dot m-junction upwards (+) or downwards (−). The changes in free energy associated with these electron transfers can be directly defined from equation (1) as

$$\begin{aligned}
\Delta F_{1\bar{1}}^{\pm}(n_1,n_2) &= (e^2 \pm 2eQ_1)/2C_1^* \pm eQ_2/C_m^* \mp eV/2,\\
\Delta F_{1\bar{2}}^{\pm}(n_1,n_2) &= (e^2 \mp 2eQ_1)/2C_1^* \mp eQ_2/C_m^* \mp eV/2,\\
\Delta F_{2\bar{1}}^{\pm}(n_1,n_2) &= (e^2 \pm 2eQ_2)/2C_2^* \pm eQ_1/C_m^* \mp eV/2,\\
\Delta F_{2\bar{2}}^{\pm}(n_1,n_2) &= (e^2 \mp 2eQ_2)/2C_2^* \mp eQ_1/C_m^* \mp eV/2,\\
\Delta F_m^{\pm}(n_1,n_2) &= (e^2 \mp 2eQ_1)/2C_1^* + (e^2 \pm 2eQ_2)/2C_2^* - (e^2 \mp eQ_1 \pm eQ_2)/C_m^*.
\end{aligned} \quad (2)$$

At temperature T, the rate of an electron transfer across any ν-junction ($\nu = 1\bar{1}, 1\bar{2}, 2\bar{1}, 2\bar{2}$ and m) is well-known [2]:

$$\Gamma_\nu^{\pm} = (e^2R_\nu)^{-1}\Delta F_\nu^{\pm}/[\exp(\Delta F_\nu^{\pm}/k_BT) - 1], \quad (3)$$

where R_ν is the tunnel resistance of the ν-junction and $\Delta F_\nu^{\pm}$ is the corresponding change in free energy defined in equation (2). In the limit of zero temperature, this expression reduces to

$$\Gamma_\nu^{\pm} = \Theta(-\Delta F_\nu^{\pm})|\Delta F_\nu^{\pm}|/e^2R_\nu, \quad (4)$$

where Θ is the step function.

Focusing on the zero-temperature case, from expressions (2) and (4), in principle, we can solve the master equation (ME) or perform Monte Carlo simulations to calculate the current and further the noise. For simple structures such as the device under study the ME method is much more efficient. Denoting by $p(i)$ the probability of the state $|i\rangle \equiv (n_1^{(i)}, n_2^{(i)})$ of the system, the ME can be written in the matrix form:

$$\mathrm{d}\hat{p}(t)/\mathrm{d}t = \hat{M}\hat{p}(t), \quad (5)$$

where $\hat{p}(t)$ is the column matrix of elements $p(i,t)$ and $\hat{M}$ is the evolution matrix with elements defined as follows: the diagonal elements,

$$\hat{M}(i,i) = -\sum_{\nu}[\Gamma_{\nu}^{+}(i) + \Gamma_{\nu}^{-}(i)]$$

and off-diagonal ones,

$$\hat{M}(i,j) = \begin{cases} \Gamma_{11}^{\pm}(j) + \Gamma_{12}^{\mp}(j) & \text{if } n_1^{(j)} = n_1^{(i)} \mp 1 \quad \text{and} \quad n_2^{(i)} = n_2^{(j)} \\ \Gamma_{21}^{\pm}(j) + \Gamma_{22}^{\mp}(j) & \text{if } n_1^{(j)} = n_1^{(i)} \quad \text{and} \quad n_2^{(j)} = n_2^{(i)} \mp 1 \\ \Gamma_{m}^{\pm}(j) & \text{if } n_1^{(j)} = n_1^{(i)} \pm 1 \quad \text{and} \quad n_2^{(j)} = n_2^{(i)} \mp 1 \\ 0 & \text{otherwise.} \end{cases} \tag{6}$$

Having stationary solutions of the ME (5) under the condition $\sum_i p(i,t) = 1$, one can calculate the stationary net current, which is the sum of two currents across two junctions $\bar{1}1$ and $\bar{2}1$ (or $\bar{1}2$ and $\bar{2}2$):

$$I = I_{11} + I_{21} = e\sum_{i}[\Gamma_{11}^{+}(i) - \Gamma_{11}^{-}(i) + \Gamma_{21}^{+}(i) - \Gamma_{21}^{-}(i)]p_{\mathrm{st}}(i), \tag{7}$$

where $p_{\mathrm{st}}(i)$ is the corresponding stationary probability.

On the other hand, to study the noise we need to know the time-dependent net current $I(t)$, which for the device under study has the form[2]:

$$I(t) = \sum_{\nu} g_{\nu} I_{\nu}(t), \tag{8}$$

where $I_{\nu}(t) = e\sum_i[\Gamma_{\nu}^{+}(i) - \Gamma_{\nu}^{-}(i)]p(i,t)$ is the time-dependent current across the ν-junction, $g_{11} = [C_m(C_{12} + C_{22}) + C_{12}(C_{21} + C_{22})]/\Sigma$, $g_{12} = [C_m(C_{11} + C_{21}) + C_{11}(C_{21} + C_{22})]/\Sigma$, $g_{21} = [C_m(C_{12} + C_{22}) + C_{22}(C_{11} + C_{12})]/\Sigma$, $g_{22} = [C_m(C_{11} + C_{21}) + C_{21}(C_{11} + C_{12})]/\Sigma$, and $g_m = (C_{11}C_{22} - C_{21}C_{12})/\Sigma$ with Σ defined in equation (1).

In order to calculate the shot noise spectrum power $S(\omega)$ of the current (8), we use the expression suggested by Korotkov [4]. This expression (equation (30) in [4]), originally written for a SET with two tunnelling junctions, can be neatly extended to the following form for the multi-junction structure of interest:

$$S(\omega) = 2\sum_{\nu} g_{\nu}^2 A_{\nu} + 4e^2 \sum_{\nu\mu} g_{\nu} g_{\mu} \sum_{ij}[\Gamma_{\nu}^{+}(i) - \Gamma_{\nu}^{-}(i)] \times B_{ij}[\Gamma_{\mu}^{+}(j|\mu^{-})p_{\mathrm{st}}(j|\mu^{-}) - \Gamma_{\mu}^{-}(j|\mu^{+})p_{\mathrm{st}}(j|\mu^{+})]. \tag{9}$$

Here, $A_{\nu} = e(I_{\nu}^{+} + I_{\nu}^{-})$ with $I_{\nu}^{\pm} = e\sum_i \Gamma_{\nu}^{\pm}(i)p_{\mathrm{st}}(i)$; the conditional probability $p(i \leftarrow j|\tau)$ for having state $|i\rangle$ at the time $t = \tau > 0$ under the condition that the state was $|j\rangle$ at an earlier time $t = 0$ obeys the same ME as for the probability $p(i,t)$; the stationary probability $p_{\mathrm{st}}(i)$ is defined as $p(i \leftarrow j|\tau \to \infty) = p_{\mathrm{st}}(i)\delta_{ij}$; $\hat{B} = \mathrm{Re}[(\mathrm{i}\omega\hat{I} - \hat{M})^{-1}]$; and $\langle j|\nu^{\pm}\rangle$ is the state obtained from the state $|j\rangle$ by transferring an electron across the ν-junction to the right $(+)$/ left $(-)$ (or upwards/downwards for the m-junction). The indices ν and μ in the first and second summations run over all tunnelling junctions in the structure under study.

Thus, once the ME has been solved, one can calculate the stationary current (7) and the noise (9). For SET, SEP or SET-Box structures this equation can be analytically solved in the case of zero temperature and at low bias of the first Coulomb staircase region, when all probabilities $p(i)$ are equal to zero except those for several particular states [6, 8, 10]. For the PDQDSs of interest (figures 1(a) and (e)), however, calculations have to be performed numerically. Results obtained for different parameter configurations are presented in the

[2] The expression (4) can be derived from the work done by the voltage source considering the individual currents $I_{\nu}(t)$ across junctions.

next section. Besides, using the conductance calculated, we can draw CB-charging diagrams (conductance versus two gate parameters, $C_{g1}V_{g1}$ and $C_{g2}V_{g2}$), which describe the charge states of system in the CB-regime. Such diagrams are also presented in parallel with the current and the noise. The study is focused on the case of zero temperature and the limit of zero-frequency noise that is most relevant to experiments.

3. Numerical results and discussion

We will begin with fully symmetric PDQDSs, when all arm-junctions are identical: $C_{11} = C_{12} = C_{21} = C_{22} \equiv C$ and $R_{11} = R_{12} = R_{21} = R_{22} \equiv R$. It is then convenient in numerical calculations to choose the elementary charge e, the arm-capacitance C and the arm-resistance R as basic units. The voltage, the current, the energy and the frequency are consequently measured in units of e/C, e/CR, e^2/C and $(CR)^{-1}$, respectively. These units will be used in discussion below.

For the fully symmetric PDQDS in figure 1(a), certainly, the only problem of interest is about how the inter-dot coupling capacitance C_m and resistance R_m affect the tunnelling process of electrons across the device. In figure 2 we present calculated results of (i) the CB-charging diagram (left column), (ii) the current I and normalized zero-frequency noise (Fano factor), $S(0)/2eI \equiv F_n$, plotted against the bias voltage V (right column), and (iii) the gate-spectroscopy of conductance G (left axis) and noise (right axis) (middle column). Here, all the results shown in the three figures in the same line come from the structures with the same capacitance C_m, which is equal to 0.01, 1 and $5C$ for the top, middle and bottom line, respectively. Besides, in each figure in the middle and right columns, two data sets are shown for structures different only in resistance R_m, $R_m = 1$ (solid lines) and $100R$ (dashed lines).

Certainly, for the fully symmetric PDQDS discussed, the current, the conductance and therefore the charging diagram should not be affected by the inter-dot resistance R_m (two currents (conductances), corresponding to two values of R_m, in each figure in the right (middle) column are coincident). So, the evolution of the charging diagram observed in the left column of figure 2 is due to varying solely the capacitance C_m. At small C_m (top line), when the inter-dot coupling is much weaker than couplings between dots and leads, electrons almost separately tunnel through the two nearly independent identical SETs that results in the Coulomb gap with a typical threshold voltage of $V_c \approx e/2C$ (figure 2(g)) and the charging diagram with rectangular cells (figure 2(a)). Correspondingly, in figure 2(d) for the same C_m the conductance shows an oscillation with a period of $\approx e$, characterizing the tunnelling through two separated QDs. As the inter-dot coupling capacitance C_m increases, each conductance peak gradually splits into two sub-peaks (figures 2(e) and (f)), leading to a deformation of rectangular diagram cells into rounded hexagons (figure 2(b)). The threshold voltage V_c is at the same time decreased (figure 2(h)). At large C_m (bottom line), when the inter-dot coupling is much stronger than couplings between dots and leads, two QDs almost merge into one. Consequently, the two sub-peaks of conductance tend to be fully separated (figure 2(f)), the diagram-cell boundaries tend to be straight lines (figure 2(c)) and the threshold voltage approaches the limiting value of $e/4C$ for a single symmetric SET with capacitances of $2C$. In the limit of very large C_m the CB-conductance gate-spectroscopy has a form like that for single dot structure, but the peak spacing is two times shorter (compared to figure 2(d)).

It is worth mentioning that the evolution of charging diagrams with respect to the inter-dot capacitance C_m, presented in figures 2(a)–(c), resembles quite well the experimental data reported by Chen *et al* in [19], where the CB-charging diagrams have been examined at various values of the inter-dot conductance. A similar experimental result has been also reported by Holleitner *et al* [20].

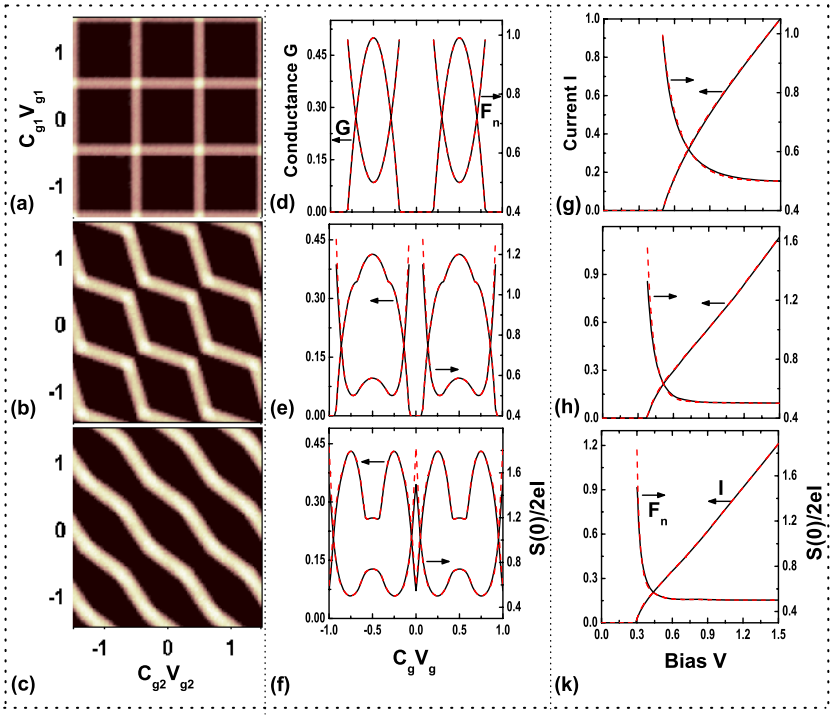

Figure 2. Charging diagrams (left column; whiteness indicates a high-conductance region), the gate-spectroscopy of conductance G (left axis) and noise (right axis) (middle column), and currents I (left axis) and Fano factors $F_n = S(0)/2eI$ (right axis) as functions of bias V (right column) for the fully symmetric PDQDS in figure 1(a) [$C_{11} = C_{12} = C_{21} = C_{22} \equiv C$; $R_{11} = R_{12} = R_{21} = R_{22} \equiv R$]. C_m is the same for all figures in the same line: $C_m = 0.01C$ for (a), (d) and (g) in the first line, C for (b), (e) and (h) in the second line, and $5C$ for (c), (f) and (k) in the last line. In the middle and right columns solid (or dashed) lines correspond to $R_m = 1$ (or $100R$). The conductance and noise gate-spectroscopies (middle column) are taken at the bias $V = 0.3$, assuming $C_{g1}V_{g1} = C_{g2}V_{g2} \equiv C_gV_g$. In this and all other figures below the voltage, the current, the conductance and the noise are measured in units of e/C, e/CR, R^{-1} and $(CR)^{-1}$, respectively.

As for the noise, comparing the noise curves in three figures in the right column of figure 2 we see that an increase in the inter-dot capacitance C_m may lead to an essential enhancement of noise in the region of biases close to the Coulomb gap threshold voltage. While, the noise is sub-Poissonian ($F_n < 1$) in figure 2(g) for $C_m = 0.01C$, it becomes super-Poissonian ($F_n > 1$) in figure 2(h) for $C_m = C$, and larger in figure 2(k). Interestingly, these figures also show that even the resistance R_m might affect the magnitude of the noise in the same region of biases. Really, in both figures 2(h) and (k) the dashed line of noise for $R_m = 100R$ rises to a value considerably higher than that for the corresponding solid line of $R_m = R$. Quantitatively, the R_m-induced noise enhancement depends somewhat on the capacitance C_m, it is stronger in the device with larger C_m. So, our study clearly demonstrates that the noise is more sensitive to the inter-dot coupling than the conductance. Note that all these effects can also be identified in figures in the middle column, where the noise shows an oscillation with the same period as the conductance. These two quantities, however, as is well known, change in opposite directions as (C_gV_g) varies so that the maximum of conductance corresponds exactly to the minimum of noise, and vice versa.

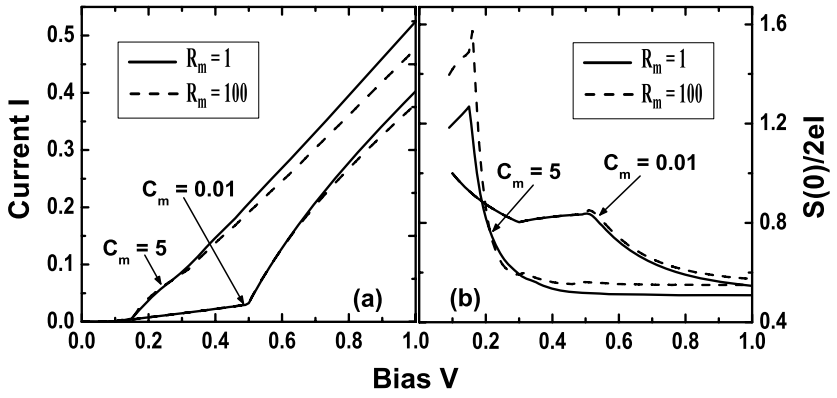

Figure 3. (a) Currents I and (b) Fano factors F_n are plotted against the bias V for the PDQDS in figure 1(a), where junction $\bar{12}$ is made different from the rest. Parameters are: $C_{11} = C_{21} = C_{22} \equiv C$, $R_{11} = R_{21} = R_{22} \equiv R$, $C_{12} = 5C$, $R_{12} = 10R$, the values of $C_m[C]$ and $R_m[R]$ are given in the figures.

Thus, we have shown that even for fully symmetric PDQDSs the inter-dot coupling may cause an essential change of CB-charging diagrams and significantly affect the magnitude of the noise. An asymmetry in arm-junction parameters can not only directly induce a change in current and noise but can also modify the relative role of inter-dot coupling. As a demonstration, we show in figure 3 the I–V curves (a) and the Fano factor (b) calculated for the structure, in which only junction $\bar{12}$ has been made different from the rest (with parameters given in the figure). An increase of R_{12} (10 times) results in a decrease of currents in figure 3 which are about two times less than corresponding currents in figure 2. Besides, the CB-threshold voltages as well as the partial currents associated with two arm-SETs are now different, giving rise to the breaking points in both I–V and F_n–V curves. By comparing two curves for the same C_m (or the same R_m), we can see also that the inter-dot coupling effect, caused by both C_m and R_m, becomes considerably stronger in figure 3 compared to figure 2 for fully symmetric structures. Both the I–V and F_n–V curves sharply change their form with varying C_m. The resistance R_m now affects not only the magnitude of the noise (see figure 3(b)) like that observed in figure 2, but also the current (see figure 3(a)). Certainly, for any structure (in figure 2 or 3) the inter-dot coupling effect is most profoundly manifested in the low bias region (close to the Coulomb gap threshold voltage), when the CB-effect is more important.

Next, we turn our attention to the structure in figure 1(e), which consists of two SETs capacitively coupled to each other, but there is no tunnelling between them. As mentioned above, such a PDQDS has been experimentally investigated in [21], where the charging diagram and the conductance associated with each QD are measured separately. Lacking exact parameter values of the structure measured, we do not attempt to make a quantitative comparison, but simply present in figure 4 the calculated results of (i) the CB-charging diagrams for dot D_1 (left column) and dot D_2 (middle column) and (ii) the gate-spectroscopy of conductance $G_{1(2)}$ (dashed lines) and normalized zero-frequency noise $S_{1(2)}(0)/2eI_{1(2)}$ (solid lines), counted for each SET (1 and 2) with respect to its gate (right column), for the structures of identical arm-junctions [$C_{11} = C_{12} = C_{21} = C_{22} \equiv C$ and $R_{11} = R_{12} = R_{21} = R_{22} \equiv R$] and with different inter-dot capacitances as given in the figures. Note that the diagrams in figures 4(b) and (e) for the structure with $C_m = C$ seem to describe well the experimental data shown respectively in figures 2(b) and (a) of [21]. Moreover, figures 4(a)–(c) and (d)–(f), on the whole, give an overview of the evolution of CB-charging diagrams of each QD with respect

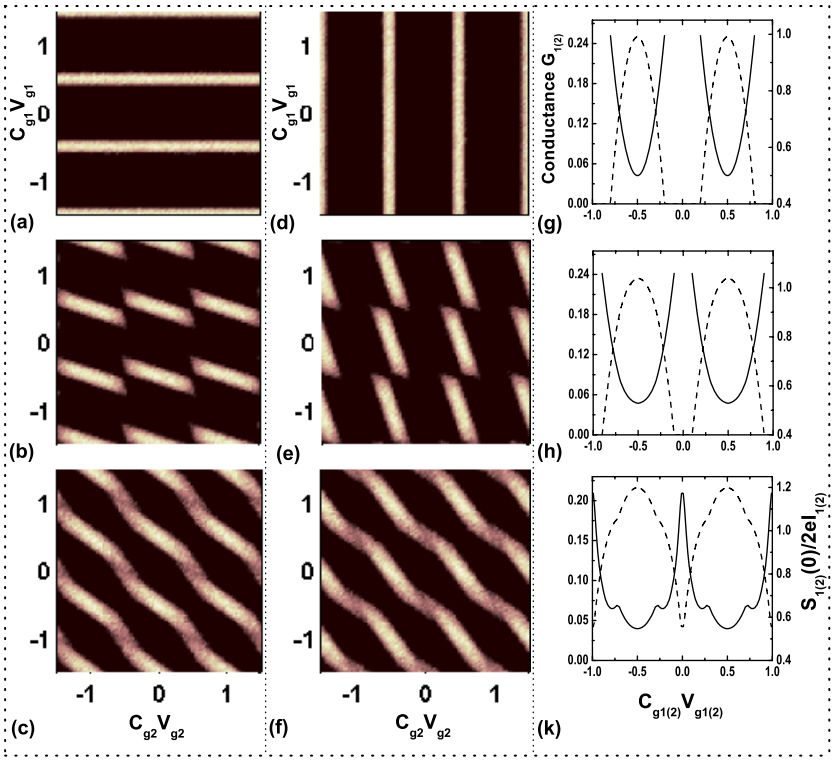

Figure 4. Charging diagrams examined separately for each QD, D_1 (left column) and D_2 (middle column) and the conductance and noise gate-spectroscopies calculated separately for each SET (right column) for the PDQDS in figure 1(e) with fully symmetric parameters [$C_{11} = C_{12} = C_{21} = C_{22} \equiv C$ and $R_{11} = R_{12} = R_{21} = R_{22} \equiv R$]. C_m is the same for all figures in the same line: $C_m = 0.01C$ for (a), (d) and (g), C for (b), (e) and (h), and $5C$ for (c), (f) and (k). The separated SET-conductances (dashed lines) and noises (solid lines) in the right column are taken at bias $V = 0.3$ and plotted versus corresponding gate parameters.

to the inter-dot coupling. The physics of such an evolution is the same as that discussed in figure 2. And, additionally, for a given device a superposition of two separated QD diagrams in figure 4 (e.g. figures 4(a) and (d) or figures 4(b) and (e)) should yield a corresponding double QD diagram like that in figure 2 (e.g. figure 2(a) or (b)). An equivalent description of the CB-evolution discussed can be also found by comparing conductance gate-spectroscopies (dashed lines) in the right column of figure 4. Here, we note that due to the symmetry of two partial SETs two conductances (or noises), associated separately with each of them, are coincident and described in these figures by a single dashed (or solid) line. In comparison with the whole device conductance gate-spectroscopies in figure 2 (when inter-dot tunnelling is allowed), the separated QD spectroscopies in figure 4 (when inter-dot tunnelling is prohibited) evolve similarly with a gradual split of conductance peaks as the capacitance C_m increases, but the tempo of change is slower.

We recall that in contrast to figure 2, all quantities presented in figure 4, including the noise gate-spectroscopies in the right column (solid lines), are separately counted for each QD. Even so, the conductances as well as the noises in these two figures, the middle column of figure 2 and the right column of figure 4, behave quite similarly towards corresponding gates. Figure 4 again demonstrates that even for the structure where there is no tunnelling between QDs and

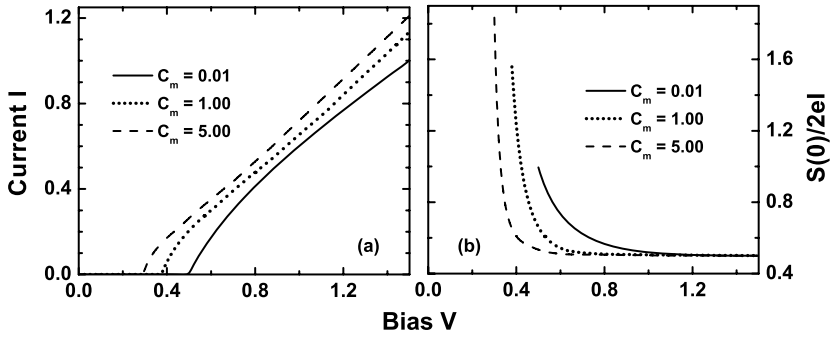

Figure 5. For the whole structure, (a) stationary net currents I and (b) Fano factors F_n are plotted against the bias V for the fully symmetric PDQDS studied in figure 4.

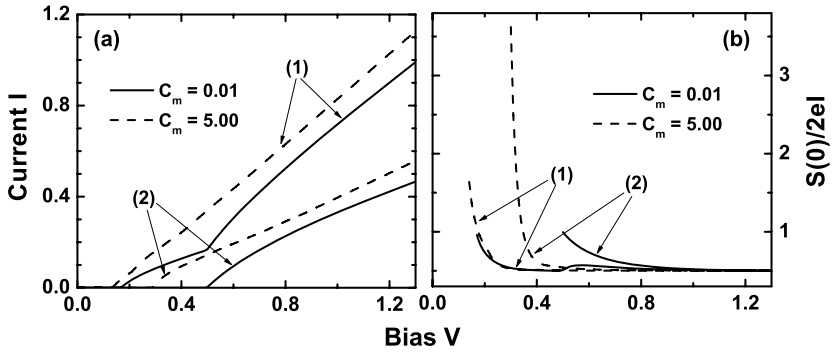

Figure 6. A continuity of figure 5, but for two particularly asymmetric parameter configurations: (1) $C_{11} = C_{12} \equiv C$, $C_{21} = C_{22} = 3C$, and all resistances are the same and equal to R and (2) $R_{11} = R_{12} \equiv R$, $R_{21} = R_{22} = 10R$, and all arm-capacitances are the same and equal to C. The values of $C_m[C]$ are given in the figures.

when two partial SETs are fully symmetric the noise is enhanced with increasing C_m and may become super-Poissonian (see figures 4(h) and (k)).

As for the whole device, we present in figure 5 the stationary net current I and the Fano factor F_n plotted versus the bias V for the same symmetric devices as those studied in figure 4. Similar to figure 2 (right column), figure 5 clearly shows an enhancement of both (a) current and (b) noise, accompanied with a narrowness of the Coulomb gap (a), as the capacitance C_m increases. In the case of strong inter-dot coupling ($C_m = 5C$) the noise is as large as $F_n \approx 1.83$, and from calculations (not shown) we learn that it may become larger with further increase in C_m.

As a continuation of figure 5, we show in figure 6 the I–V and F_n–V curves for two particular configurations of the device in figure 1(e), when two partial SETs are not identical (with parameters given in the figure). An increase of two arm-junction capacitances in one of SETs by only three times, keeping resistances symmetric (see curves (1) in figure 6(a)) leads to a considerable narrowing of Coulomb gaps compared to figure 5. On the other hand, due to an increase of two arm-junction tunnelling resistances in one of the SETs (by 10 times), keeping capacitances symmetric (see curves (2)), the magnitude of the current becomes almost two times less, whereas the Coulomb gap thresholds remain certainly unchanged (in comparison with figure 5(a)). Quantitatively, with respect to the current, the inter-dot coupling effect in

figure 6(a) is about the same as in figure 5(a) for fully symmetric structures, but with respect to the noise the effect is stronger. For the case when two partial SETs are different only in tunnel resistances and the inter-dot coupling is strong (see the dashed line for $C_m = 5C$ in figure 6(b)), the noise is as large as $F_n \approx 3.62$ (compared to the corresponding value $\approx$1.83 in figure 5(b)). Thus, our study again shows that in comparison with the conductance, the noise is more sensitive to not only the inter-dot coupling but also the parameter asymmetry.

All results reported above are focused on PDQDSs that are symmetric or not far from symmetric. In the limiting case of strong asymmetric structures, such as those studied in [6, 10], the I–V curves may exhibit NDC regions (or even multi-Coulomb gaps) and the noise may be very large.

4. Conclusion

We have systematically examined the charging diagram and calculated the current and noise in parallel double metallic quantum dot structures in the CB-regime. It was shown that the evolution of charging diagrams obtained by changing only the inter-dot capacitance describes quite well the experimental data reported for structures with [18–20] as well as without [21] tunnelling between QDs. The inter-dot capacitance and resistance also strongly affect the noise, making it super-Poissonian even in fully symmetric structures. The stronger the electrostatic coupling between dots the larger the noise may become. An asymmetry in structure parameters, enhancing the influence of inter-dot coupling, may produce a variety of current and noise magnitudes as well as their bias-dependent behaviours. In the limit, the asymmetry may cause a negative differential conductance and/or a very large noise. For all structures studied, in comparison with the conductance, the noise is shown to be more sensitive to changes in device parameters and therefore it can provide more information on the physical nature of the problem. In particular, for fully symmetric PDQDSs when the stationary current does not depend on the inter-dot resistance at all, only the noise can give useful information about the role of this resistance. So, the present results suggest a key role for noise measurements in attempting to understand the finer points of electron tunnelling processes in parallel double QD structures.

The study has been carried out at zero temperature. Though, in principle, any finite temperature can destroys the CB-effect, all results discussed should remain qualitatively relevant to the case when the temperature is still much lower than the charging energy.

Acknowledgments

One of the authors (VLN) thanks Professor H T Diep for kind hospitality at the Université de Cergy-Pontoise (France), where this paper has been written. This work was supported by the Ministry of Science and Technology (Vietnam) via the Fundamental Research Program (project no. 402306).

References

[1] For a review, see Grabert H and Devoret M H (ed) 1991 *Single Charge Tunneling* (*NATO ASI Ser. B*) (New York: Plenum)
[2] Averin D V and Likharev K K 1991 *Mesoscopic Phenomena in Solids* ed B L Altshuler, P A Lee and R A Webb (Amsterdam: North-Holland)
[3] Hershfield S, Davies J H, Hyldgaard P, Stanton C J and Wilkins J W 1993 *Phys. Rev.* B **47** 1967
[4] Korotkov A N 1994 *Phys. Rev.* B **49** 10381
[5] Blanter Ya M and Buttiker M 2000 *Phys. Rep.* **336** 1

[6] Hung Nguyen V, Lien Nguyen V and Nam Nguyen H 2005 *J. Phys.: Condens. Matter* **17** 1157
[7] Aghassi J, Thielmann A, Hettler M H and Schon G 2006 *Phys. Rev.* B **73** 195323
[8] Hung Nguyen V, Lien Nguyen V and Dollfus P 2005 *Appl. Phys. Lett.* **87** 123107
[9] Heij C P, Dixon D C, Hadley P and Mooij J E 1999 *Appl. Phys. Lett.* **74** 1042
[10] Hung Nguyen V and Lien Nguyen V 2006 *Phys. Rev.* B **73** 165327
[11] Chi F and Li S S 2006 *J. Appl. Phys.* **99** 043705
Chi F and Li S S 2005 *J. Appl. Phys.* **97** 123704
[12] Apel V M, Davidovich M A, Chiappe G and Anda E V 2005 *Phys. Rev.* B **72** 125302
[13] Ding G-H, Kim C K and Nahm K 2005 *Phys. Rev.* B **71** 205313
[14] Tanaka Y and Kawakami N 2005 *Phys. Rev.* B **72** 085304
[15] DiVincenzo D P 2005 *Science* **309** 2173
[16] Petta J R *et al* 2005 *Science* **309** 2180
[17] Engel H-A and Loss D 2002 *Phys. Rev.* B **65** 195321
[18] Adourian A S, Livermore C, Westervelt R M, Campman K L and Gossard A C 1999 *Appl. Phys. Lett.* **75** 424
[19] Chen J C, Chang A M and Melloch M R 2004 *Phys. Rev. Lett.* **92** 176801
[20] Holleitner A W, Blick R H and Ebert K 2003 *Appl. Phys. Lett.* **82** 1887
Blick R H *et al* 2003 *Physica* E **16** 76
[21] Chan I H, Fallahi P, Westervelt R M, Maranowski K D and Gossard A C 2003 *Physica* E **17** 584
Chan I H *et al* 2002 *Appl. Phys. Lett.* **80** 1818